Quenching of Photoluminescence in Conjugates of Quantum Dots and Single-Walled Carbon Nanotube

Vasudevanpillai Biju,*,† Tamitake Itoh,† Yoshinobu Baba,†,‡ and Mitsuru Ishikawa†

Nano-Bioanalysis Team, Health Technology Research Center, National Institute of Advanced Industrial Science and Technology (AIST), 2217-14 Hayashi-cho, Takamatsu, Kagawa 761-0395, Japan

Received: September 5, 2006; In Final Form: October 13, 2006

Development of quantum dot (QD) based device components requires controlled integration of QDs into different photonic and electronic materials. In this regard, introduction of methods for regular arrangement of QDs and investigation of properties of QD-based assemblies are important. In the current work we report (1) controlled conjugation of CdSe−ZnS QDs to sidewall-functionalized single-walled carbon nanotube (SWCNT) templates (2) and the effect of conjugation of QDs to SWCNT on the photoluminescence (PL) properties of QDs. We identified that PL intensity and lifetime of QDs are considerably reduced after conjugation to SWCNT. The origin of the quenching of the PL intensity and lifetime was discussed in terms of Förster resonance energy transfer (FRET). FRET involves nonradiative transfer of energy from a photoexcited QD (energy donor) to a nearby SWCNT (energy acceptor) in the ground state. This was examined by varying the density of QDs on SWCNT and conjugating smaller and bigger QDs to the same SWCNT. We estimated the FRET efficiency in QD−SWCNT conjugates from the quenching of the PL intensity and lifetime and identified that FRET is independent of the density and type of QDs on SWCNT but inherent to QD−SWCNT conjugates.

Introduction

Nanodots, nanowires, and nanotubes of metals, semiconductors, and organic materials are promising building blocks for constructing hybrid structures for nanotechnology.[1−13] Controlled integration of nanoscale materials into hierarchical structural forms is inevitable for advancing nanoscale scientific research during the design of novel hybrid materials and tailoring of material properties at the nanoscale. [1, 3, 9−11, 14−28] In this regard, quantum dots are important materials.[1,15,29−33] Fabrication of QD-based device components demands their controlled integration into other photonic and electronic materials. Therefore, introduction of methods for controlled and regular arrangements of QDs in one, two, and three dimensions has great potential. Among different QDs, CdSe and CdSe−ZnS are specifically interesting for their unique optical and electronic properties.[2,5,29,34−45] Despite the incredible advancements in the synthesis and understanding of the structural, optical, and electronic properties of QDs, development of methods for controlled arrangements of QDs and understanding the optical properties of QD-based nanofabricated structures are not explored enough. Although bottom-up techniques such as covalent conjugation and self-assembly and top-down lithography techniques are widely used for integrating QDs into various structural forms, a general strategy of controlled linear arrangements of colloidal QDs is not available. Considering small diameters and structural and chemical stabilities, functionalized single-walled carbon nanotubes (SWCNTs) are promising templates for linear arrangements of QDs.

Chemical modifications of sidewall and ends of carbon nanotubes are useful for preparing carbon nanotube (CNT) templates. When CNTs are directly conjugated to other materials, surface defect states on CNT dictate the location and density of conjugation. Generally, defect sites on sidewall and end-oxidized carboxylic groups are useful for conjugation of QDs to CNTs.[19,46−55] In-situ growth of QDs on CNTs[48] and micelle-mediated electrostatic labeling of QDs on SWCNT[56] are other methods for preparing QD−CNT conjugates. Different methods for functionalization of CNTs and conjugation of nanoparticles to functionalized CNTs are discussed in a recent review article.[57] However, from time-to-time preparations of QD−SWCNT conjugates following the existing methods provided inhomogeneous distributions of QDs at ends, junctions, and defect sites on CNTs. Furthermore, controlled and linear arrangements of QDs on CNTs and the effect of conjugation of QDs to CNTs on the photoluminescence (PL) properties of QDs were not investigated in detail. In the current work, we used a known method, an addition reaction of *p*-nitrobenzenediazonium salt,[58,59] for the sidewall functionalization of SWCNT. The sidewall-functionalized SWCNT was conjugated with two types of QDs. Interestingly, we observed that the PL intensities and lifetimes of QDs were considerably reduced after conjugation to SWCNT. In order to understand the origin of the reduced PL intensity and lifetime of QDs, two types of samples were prepared: (1) QD−SWCNT conjugates with different density of QDs and (2) QD−SWCNT conjugates with two types of QDs, CdSe−ZnS QDs having PL emission maximums at 585 (QD585) and 605 nm (QD605), attached to the same SWCNT. On the basis of the quenching of the PL intensities and lifetimes, control experiments, and literature reports, we assigned a Förster resonance energy-transfer (FRET) process from QD to SWCNT in the QD−SWCNT conjugates.

FRET involves transfer of energy from a photoexcited donor to a ground-state acceptor chromophore in the proximity of the donor. The transfer of energy occurs nonradiatively, without radiation of a photon from a donor and reabsorption by an

* To whom correspondence should be addressed. Phone: (81) 87-869-3558. Fax: (81) 87-869-4113. E-mail: v.biju@aist.go.jp.

† Nano-Bioanalysis Team.

‡ Department of Applied Chemistry Graduate School of Engineering, Nagoya University, Furo-cho, Chikusa-ku, Nagoya 464-8603, Japan.

10.1021/jp0657890 CCC: $33.50 © 2006 American Chemical Society
Published on Web 12/01/2006

acceptor, by coupling between dipoles of a donor and an acceptor. There are at least three basic requirements for FRET to occur: (1) overlap between the emission spectrum of a donor and absorption spectrum of an acceptor, (2) coupling between donor and acceptor transition dipoles, and (3) close proximity of donor and acceptor. According to the Förster formalism, the rate of energy transfer in a donor−acceptor system which fulfills the above requirements can be presented using eq 1[60]

$$k_T = \frac{1}{\tau_d}\left(\frac{R_0}{r}\right)^6 \quad (1)$$

where τ_d is the radiative lifetime of a donor in the absence of an acceptor, R_0 is the Förster distance at which the efficiency of energy transfer is 50%, and r is the donor-to-acceptor distance. From eq 1 it is apparent that the donor−acceptor distance (r) is an important parameter for efficient energy transfer. Generally, $r \leq 100$ Å is standard for FRET.[60,61] Although numerical values of τ_d and r can be obtained from fluorescence/PL measurements for a known system of donor and acceptor, estimation of R_0 requires different parameters including spectral overlap integral, orientation of donor−acceptor dipoles, refractive index of the medium, and fluorescence quantum efficiency of donor. On the other hand, measurement of FRET efficiency, which is an estimation of the number of photons transferred to an acceptor relative to the number of photons absorbed by a donor, is a more direct method. FRET efficiency can be estimated using eq 2[60]

$$E = 1 - \left(\frac{\tau_{da}}{\tau_d}\right) = 1 - \left(\frac{\phi_{da}}{\phi_d}\right) \quad (2)$$

where τ_{da} and τ_d are the fluorescence lifetimes of a donor in the presence and absence of an acceptor and ϕ_{da} and ϕ_d are the fluorescence quantum efficiencies of a donor in the presence and absence of an acceptor. The presence of FRET in a donor−acceptor system can be identified from quenching of both fluorescence intensity and lifetime of the donor. After FRET occurs, the acceptor relaxes to the ground state either radiatively or nonradiatively.

Among the unique optical properties of QDs, high PL quantum efficiency, photostability, and high molar extinction coefficient make QDs promising donors during the construction of FRET systems. On the other hand, absorption spectra of QDs extending in the UV−vis regions make them less attractive acceptors for FRET systems. The significance of QDs as efficient donors and acceptors of FRET was recently reviewed by Mattoussi and co-workers.[61] When QDs without a protecting polymer shells are close-packed, FRET is possible from smaller to bigger QDs. This is due to the small diameter of the core and core−shell QDs. However, FRET from smaller to larger QDs is unlikely to occur in core−shell QDs with thick protective layers. Therefore, core−shell QDs with protective layers are not attractive donor−acceptor pairs for a FRET system but can be efficient donors when used in conjunction with small acceptor chromophores in the proximity. Here, we report the preparation of QD−SWCNT conjugates and the steady-state and time-resolved PL properties of QDs in the conjugates. We observed considerable quenching of the PL intensity and lifetime of QDs after conjugation to SWCNT. The origin of the quenching of the PL intensity and lifetime was investigated in terms of FRET by preparing QD−SWCNT conjugates with varying density of QDs on SWCNT and smaller and bigger QDs on the same SWCNT. On the basis of the principles underlying FRET, FRET in QD-based systems, control experiments, and having observed reduced PL intensity and lifetime of QDs in QD−SWCNT conjugates, we propose that FRET from QDs to SWCNT is involved in the QD−SWCNT systems.

Experimental Section

Materials. The QD−SWCNT conjugates were prepared by reacting biotinylated-SWCNT with commercial streptavidin-QD conjugates. SWCNT was purchased from Aldrich and functionalized with biotin following a literature method. We used two types of commercial streptavidin-QD conjugates [PL emission maxima ≈ 585 (QD585) and 605 nm (QD605)] for preparing QD−SWCNT conjugates. The streptavidin-QD conjugates were purchased from Quantum Dot Corp. (now Invitrogen, Carlsbad, CA). The streptavidin molecules present on the surface of polymer coated CdSe−ZnS QDs are powerful agents for linking different molecules to QDs through streptavidin−biotin coupling. Stock solutions for PL measurements, AFM imaging, and Raman measurements were prepared by dispersing QD−SWCNT conjugates in Milli-Q water (Milli-Pore Corp., Billerica, MA) to solutions of required concentrations. Samples for AFM imaging were prepared by incubating (10 min) QD−SWCNT conjugate solutions on freshly cleaved mica plates followed by gentle washing using Milli-Q water and drying in air. Samples for Raman spectral analysis and fluorescence microscopy were prepared by placing 50 μL of QD−SWCNT conjugate solutions on slide glasses followed by spin coating (uniform distribution and drying of a small fraction of a sample solution by spinning) at 3000 rpm for 30 s. Concentrations of QD−SWCNT conjugates used for the sample preparations were equivalent to 100 nM QD solution (for Raman spectroscopy) and 1 nM QD solution (for fluorescence imaging).

Instruments Used. Absorption and emission spectra were recorded in a Hitachi-4100 spectrophotometer and a Hitachi-4500 spectrofluorometer, respectively. Topography images of QD−SWCNT conjugates were obtained using a MFP-3D atomic force microscope (AFM, Asylum Research, Santa Barbara, CA). Tapping-mode AFM images were collected in air using reflective-aluminum-coated ultrasharp (radius of curvature < 10 nm) silicon microcantilevers (Olympus, Tokyo). The cantilevers used were ∼160 μm long and had a spring constant of ∼42 N/m and a resonance frequency of ∼300 kHz. Field emission scanning electron micrographs (FESEM) were recorded using a JEOL JSM-6700F system. Fluorescence and Raman spectra were recorded in an inverted optical microscope (Olympus IX70) using an Andor spectrometer (Andor Technology, Tokyo) by exciting at 457 (fluorescence) and 633 nm (Raman). Fluorescence images of QD−SWCNT conjugates were recorded using a wide-field video microscopy system. A correlated AFM-optical microscope (Olympus-IX70) system equipped with band filters for orange and red fluorescence, a 100X objective (Olympus-UMPlanFl, NA 0.95), an image intensifier (Video Scope VS4−1845), and a CCD camera (Hamamatsu-C5985) were used. The excitation source used for fluorescence imaging was the second harmonics (532 nm) of a cw Nd:YAG laser (Coherent DPSS). PL lifetimes of QD−SWCNT conjugates were measured using an assembly of a polychromator (Chromex, model 250IS) and a photon-counting streak-scope (Hamamatsu-C4334). The excitation source used for lifetime measurements was 400 nm pulses (150-fs) generated from the SHG crystal of an optical parametric amplifier (Coherent OPA 9400). The OPA was pumped at a 200 kHz rate by a regenerative amplifier (Coherent RegA 9000) which was seeded by a mode-locked Ti:Sapphire laser (Coherent Mira 900F). The PL from QD−

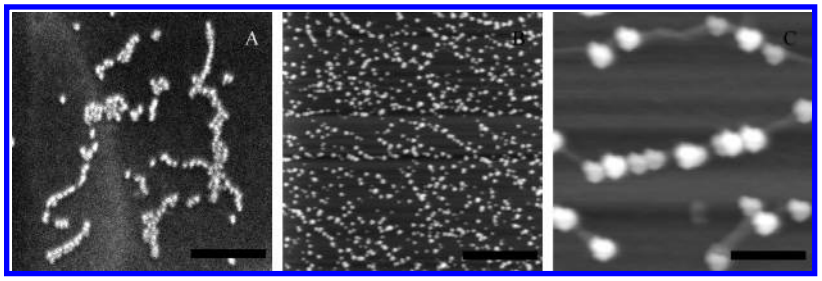

Figure 1. (A) FESEM image of QD−SWCNT conjugates. (B) Tapping-mode AFM height image of QD605-SWCNT conjugates. (C) An enlarged portion of a zoom-in and scanned AFM height image of QD−SWCNT conjugates showing specific conjugation of QDs to biotinylated-SWCNTs. The scale bars are 250 nm (A), 2 μm (B), and 100 nm (C).

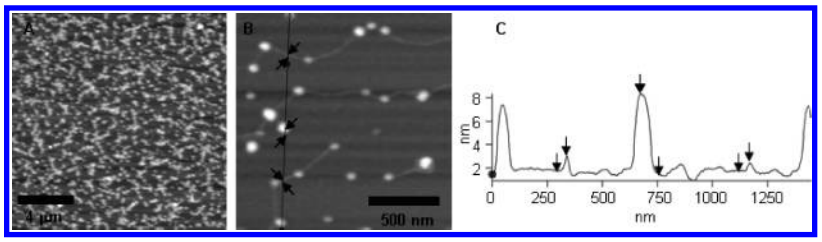

Figure 2. Tapping-mode AFM height images of QD605-SWCNT conjugates prepared by reacting 200 (A) and 10 nM (B) QD605 with 10 μg/L solutions of biotinylated-SWCNT. Zoom-in and scanned image is presented in (B) to identify spatial separation of QDs. (C) Surface profile of (B). The arrows in (B) and (C) show locations and heights of QDs and SWCNTs.

SWCNT samples was filtered through a 570 nm long-pass filter and focused at the entrance slit of the polychromator.

Preparation of QD−SWCNT Conjugates. QD−SWCNT conjugates were prepared via biotin−streptavidin coupling between biotinylated-SWCNT and streptavidin-QDs. We used three-step reactions for the preparation of biotinylated-SWCNT. Although several methods are available for sidewall functionalization of SWCNT, we followed an addition reaction of aromatic diazonium salt to SWCNT developed by Dyke and Tour[58,59] with slight modifications. In a typical reaction *p*-nitrobenzenediazonium tetrafluoroborate was reacted at 10 °C for 96 h with SWCNT, which was stabilized in sodium dodecyl sulfate (SDS) micelles. Dispersion of SWCNT in surfactants such as SDS and sodium dodecylbenzene sulfate (SDBS) is standard for preserving SWCNT in unbundled form. The prolonged reaction was helpful for excessive sidewall functionalization of SWCNT into its *p*-nitrobenzene derivative. The *p*-nitrobenzene derivative was separated and purified by column chromatography and further reduced using $NaBH_4$ into *p*-aniline derivative. The reduction reaction was carried out in dry DMSO. We observed that the *p*-aniline-conjugated SWCNT is soluble in aqueous solutions, probably due to excessive sidewall functionalization[58,59] and formation of quaternary ammonium salt. Increasing the distribution of specific defect sites on the sidewall of SWCNT by introducing a large number of functional groups was helpful to arrange QDs on SWCNT templates. In the current work, we prepared three types of QD−SWCNT conjugates by coupling QD585 and QD605 to the *p*-aniline derivative of SWCNT through biotin−*N*-hydroxysuccinimide ester (biotin−NHS-ester), a heterobifunctional cross-linker widely used in bioconjugate reactions. Here, the aniline group was first coupled to the NHS ester, and the biotin group was conjugated to the streptavidin moiety on QDs in a successive step. The three types of QD−SWCNT conjugates prepared in the current work were QD585-SWCNT, QD605-SWCNT, and a mixed conjugate of QD585 and QD605 on the same SWCNT. Also, the density of QD conjugation on SWCNT was varied by reacting QD605 solutions having different concentrations (200, 100, 50, and 10 nM) with biotinylated-SWCNT solutions (10 μg/L). For preparation of the mixed conjugate, an emission intensity matched (at 585 and 605 nm) QD solution containing QD585 and QD605 was reacted with biotinylated-SWCNT.

Characterization of QD−SWCNT Conjugates. Formation of the QD−SWCNT conjugates was identified from AFM, FESEM, and fluorescence imaging. Also, the conjugates were characterized using correlated fluorescence and Raman spectral analyses. Typical FESEM and tapping-mode AFM height images of QD605-SWCNT conjugates are shown in Figure 1A−C. We used AFM and FESEM imaging for technical reasons. The linear arrays of QDs observed in Figure 1A and B are not due to simple line up of QDs without conjugation to biotinylated-SWCNT. This was confirmed from high-resolution AFM imaging of QD−SWCNT conjugates. A zoom-in and scanned AFM image of QD605-SWCNT conjugates is shown in Figure 1C. Also, nonspecific line up of QDs in the absence of SWCNT/biotinylated-SWCNT was ruled out based on FESEM and AFM imaging. Therefore, we consider that the structures in Figure 1A−C are QD605-SWCNT conjugates. We examined the effect of the concentration of QD solutions on the distribution of QDs on SWCNT. For this we varied the concentration of QD605 employed in the conjugation reaction. AFM images of QD−SWCNT samples prepared from 200, 100, 50, and 10 nM QD605 solutions were useful for identifying the distribution of QDs on SWCNT. The concentration (10 μg/L) of biotinylated-SWCNT was kept constant in the conjugation reactions. The constant concentration of biotinylated-SWCNT was helpful to understand the effect of QD concentration on the distribution of QDs in QD−SWCNT conjugates. Typical AFM height images of QD−SWCNT conjugates prepared from 200 and 10 nM solutions of QD605 and 10 μg/L solution of biotinylated-SWCNT are shown in Figure 2A and B. Heights of QDs and SWCNTs are shown in a surface profile (Figure 2C) of Figure 2B. Also, we identified that free QDs and SWCNTs and nonspecific aggregates of QDs and SWCNTs were minimized under the selected concentrations of QDs and biotinylated-SWCNT for the conjugation reactions. On the other hand, when concentrations of QD ($\geq$300 and $\leq$10 nM) and biotinylated-SWCNT ($\geq$25 and $\leq$0.5 μg/L) solutions were above and below a certain range, clusters of (at higher concentrations in the above ranges) and isolated (at lower concentrations in the above

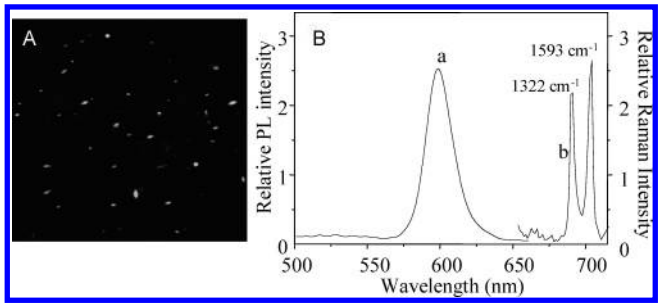

Figure 3. (A) PL image (60 μm × 60 μm) of QD605-SWCNT conjugates. The sample was excited with a circular polarized 457 nm cw laser, and the PL signals were collected using a 30 nm band-pass filter for 605 nm. (B) Characteristic PL (a) and Raman (b) bands of QD605-SWCNT conjugates collected from the same sample area. The PL spectrum was obtained by exciting at 457 nm, and the Raman spectrum was obtained by exciting at 633 nm. The spectra were collected from a small sample area using a 10 μm slit.

ranges) QDs and SWCNTs were observed. From FESEM and AFM images we identified that the QD−SWCNT conjugates were formed irrespective of the concentration of QDs, and the density of QDs in the QD−SWCNT conjugates can be varied by changing the concentration of QD solutions.

In addition to the FESEM and AFM images, PL image and correlated PL and Raman spectra were useful to characterize the QD−SWCNT conjugates. For this, the PL image of a QD605-SWCNT sample was first observed in an optical microscope. A typical PL image of a low density of QD605-SWCNT conjugates is shown in Figure 3A. The fluorescence image was collected through a 30 nm band-pass filter. The sample for PL imaging was prepared by spin coating a dilute solution of QD605-SWCNT conjugates on a slide glass. Slightly elongated PL spots in Figure 3A are understandable in terms of linear structures of QD- SWCNT conjugates (Figure 1). Samples for PL and Raman spectral analyses were prepared under the same conditions as in the case of a sample imaged in Figure 1B. PL and Raman scattering signals were collected from a small sample area using a 10 μm slit. A characteristic PL spectrum of QD605 and Raman scattering bands of functionalized SWCNT from the same QD605-SWCNT conjugates are shown in traces a and b, respectively, in Figure 3B. In conjunction with the FESEM and AFM images, the coexistence of a PL band centered at 605 nm and disorder (Raman shift = 1322 cm^{-1}) and tangential breathing mode (Raman shift = 1593 cm^{-1}) Raman bands of functionalized SWCNT[58,59] confirmed the formation of QD−SWCNT conjugates. Although collective measurements of PL and Raman spectra were made on QD−SWCNT conjugates present in the selected slit area of 10 μm, contributions of nonconjugated QDs and SWCNTs to the spectra were minimized under the selected conditions of sample preparation. The Raman shifts and relative intensities of the two characteristic Raman bands (Raman shift = 1322 and 1593 cm^{-1}) of QD−SWCNT conjugates are comparable to the disorder and tangential breathing mode bands reported for functionalized SWCNTs.[58,59] From the relative intensities (~0.95:1) of the Raman bands we consider that the degree of sidewall functionalization of SWCNT in the current work is comparable to that reported in ref 58.

Results and Discussion

We observed decreased PL intensities of QD585 and QD605 in the QD−SWCNT conjugates compared to the PL of QDs before conjugation to SWCNT. The PL quantum efficiencies of QD585 and QD605 were lowered by 33.6% and 31.7%,

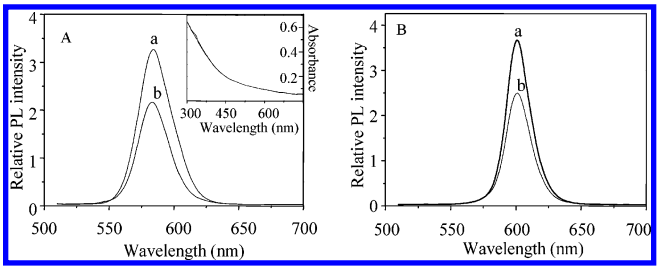

Figure 4. (A) PL spectra of (a) QD585 in the presence of aniline-functionalized SWCNT and (b) QD585-SWCNT conjugates. (B) PL spectra of (a) QD605 in the presence of aniline-functionalized SWCNT and (b) QD605-SWCNT conjugates. (Inset) absorption spectra of aniline-functionalized SWCNT and biotinylated-SWCNT; the spectra are identical.

respectively. Typical PL spectra of QD585-SWCNT and QD605-SWCNT conjugates are shown in traces b in Figure 4A and B. The PL spectra of QDs in the presence of aniline-functionalized SWCNT are also shown in Figure 4A and B (traces a) for comparison. We used aniline-functionalized SWCNT for compensating the absorbance of SWCNT; aniline-functionalized SWCNT does not bind with QDs, which was confirmed from AFM and FESEM images. Absorption spectra of SWCNT before (aniline-functionalized SWCNT) and after (biotinylated-SWCNT) biotinylation are shown in the inset of Figure 4A. It may be noted that the absorbences of SWCNT at the excitation wavelength (540 nm) before and after biotinylation are essentially the same; therefore, it is difficult to distinguish between the two spectra. The absorption spectra shown in the inset of Figure 4A is common to Figure 4A and B. The structureless absorption in the UV−vis−NIR region is characteristic to functionalized SWCNTs.[58,59] Also, the concentrations of QDs involved in the measurements of spectra a and b were essentially the same in Figure 4A and B. Therefore, the decreased PL intensities of QD585 and QD605 in QD−SWCNT are due to conjugation to SWCNT. We considered different possibilities for the decreased PL intensities of QDs in QD−SWCNT conjugates including (1) FRET from QDs to SWCNT and (2) FRET from smaller to bigger QDs in the QD−SWCNT conjugates. We ruled out a possibility that FRET from QDs to the functional groups on SWCNT is involved in PL quenching of QDs; the functional groups on SWCNT absorb light in the UV region and do not overlap with the PL spectra of QDs.

We consider that the decreased PL intensities of QD585 and QD605 in the QD−SWCNT conjugates are due to FRET from QD to SWCNT. On the basis of the Förster formalism (eq 1), there are at least two supporting points for our consideration that FRET from QD to SWCNT is involved in the PL quenching of QDs: (1) the distance between a QD and the surface of SWCNT is less than 100 Å (Figure 5A) and (2) good overlap between PL spectrum of QDs (QD585 and QD605) and absorption spectrum of SWCNT. The radius of streptavidin-QDs is ~75 Å. Also, the calculated length of the spacer between QDs and SWCNT in QD−SWCNT conjugates is 16.1 Å. The possible distances between different chromophores and fluorophores in QD−SWCNT conjugates are shown in Figure 5. The energy-minimized structure of the spacer is also shown in Figure 5. Using eq 2 and the decreased PL quantum efficiencies of QD585 (66.4%) and QD605 (68.3%) in QD−SWCNT conjugates (Figure 4) we estimated the FRET efficiencies. The FRET efficiencies are 0.34 in QD585-SWCNT conjugates and 0.32 in QD605-SWCNT conjugates. The slight difference between the FRET efficiencies is probably due to different sizes of QD585 and QD605; the smaller size of QD585 probably provided higher FRET efficiency in QD585-SWCNT conju-

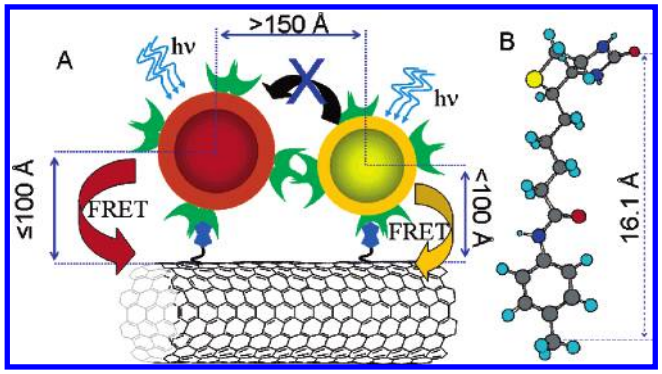

Figure 5. (A) Schematic presentation of a QD−SWCNT conjugate structure containing QD585 (smaller) and QD605 (bigger) and the possible distances between energy donors and acceptors. The average diameter of QDs is ∼150 Å. (B) Energy-minimized structure of the spacer between QDs and SWCNT.

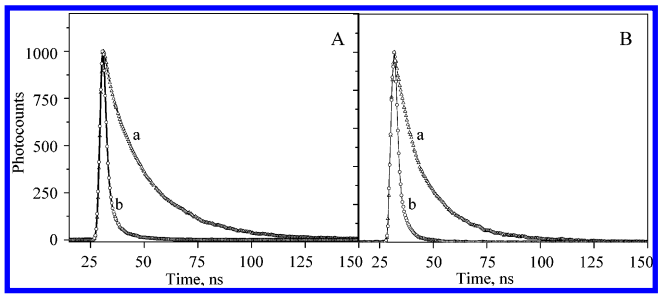

Figure 6. (A) Nanosecond PL decays of QD585 (a) and QD585-SWCNT (b) conjugates. Nanosecond PL decays of QD605 (a) and QD605-SWCNT (b) conjugates. All samples were excited at 400 nm, and the PL signals were collected though a 570 nm long-pass filter.

gates. We consider that the flexible nature of the spacer between QDs and SWCNT provided random orientations of QDs in QD−SWCNT conjugates. These random orientations probably provided coupling between the dipole moments of several QDs with that of SWCNT; the dipole moments may not always be coaxial though. The low values of FRET efficiencies in QD−SWCNT conjugates are probably due to ensemble-averaged effects of the coupling between dipole moments of SWCNT and randomly oriented QDs.

We confirmed the above possibility of FRET in QD−SWCNT conjugates from time-resolved PL measurements. QD585 and QD605 in the QD−SWCNT conjugates showed considerably reduced PL lifetimes compared to the PL lifetimes of QDs before conjugation to SWCNT. Nanosecond PL decays of QD585-SWCNT and QD605-SWCNT conjugates are shown (traces b) in Figure 6A and B, respectively. The decay profiles of QD585 and QD605 before conjugation to SWCNT are also shown (traces a) in Figure 6A and B, respectively. The decays of all the samples were multiexponential and fitted using the second-order equation. The lifetimes (τ) of fast and slow decays of QD585-SWCNT and QD605-SWCNT conjugates are $\tau_1 =$ 1.83 ns and $\tau_2 =$ 10.85 ns and $\tau_1 =$ 1.51 ns and $\tau_2 =$ 7.75 ns, respectively. Considering that the decays are multiexponential in nature, we estimated the average lifetimes. The average lifetimes (τ_{av}) of QD585-SWCNT and QD605-SWCNT are 2.01 and 1.87 ns, respectively. On the other hand, the average PL lifetimes of QD585 and QD605 before conjugation to SWCNT were 22.13 and 15.01 ns, respectively. Using the average lifetime values in eq 2 we estimated the FRET efficiencies of the QD−SWCNT conjugates. The FRET efficiencies are 0.91 for QD585-SWCNT conjugates and 0.88 for QD605-SWCNT conjugates. The values of FRET efficiencies estimated from the PL intensity and lifetime measurements showed large discrepancies. According to eq 2, the FRET efficiencies estimated from the quenching of both the PL quantum efficiencies and lifetimes are expected to be equivalent. Therefore, we consider that the decreased PL lifetimes of QD−SWCNT conjugates observed in the current work is contributed by not only FRET but also a factor that controls the stability of excitons in QDs. Part of the quenching of the PL lifetimes in QD−SWCNT conjugates is contributed by a fast radiative transition which can be accounted for only in terms of an electronic and a hydrophobic environment provided by SWCNT to QDs. If the quenching of the PL lifetime is contributed only by a nonradiative process, an equal effect is expected in the PL intensity also. However, this explanation for the quenching of the PL lifetimes of QDs is difficult to discuss further due to the presence of protective ZnS and polymer shells on QDs. A detailed investigation is underway in our laboratory regarding a correlation between the chemical environment and PL properties of QDs. On the basis of the quenching of the PL quantum efficiencies, good overlap between the absorption spectrum of SWCNT and the PL spectra of QDs, the distance between SWCNT and QDs in QD−SWCNT conjugates, the quenching of the PL lifetimes, and the literature reports on FRET, we propose that FRET from QDs to SWCNT is present in the QD−SWCNT conjugates.

The second possibility for quenching of the PL quantum efficiencies and lifetimes of QDs in QD−SWCNT conjugates is FRET from smaller to bigger QDs. This possibility was under consideration that a QD sample always contains smaller and bigger QDs, although the size distribution is narrow. It is widely known that the quantum confinement effect provides size-dependent absorption and PL spectral characteristics to QDs.[36] In other words, the absorption and emission spectra of larger QDs are red shifted compared to the smaller ones, i.e., the absorption spectrum of larger QDs overlaps with the PL spectrum of smaller QDs in a sample. Therefore, the excitation energy of a smaller QD can nonradiatively be transferred to a larger QD in the proximity. This satisfies one of the conditions of FRET from smaller to larger QDs in QD−SWCNT conjugates. However, based on the theoretical background of FRET and control experiments, we ruled out the possibility that FRET from QD to QD is involved in the QD−SWCNT conjugates. According to the Förster formalism (eq 1) and previous reports,[60,61,63,64] FRET is significant only when the distance between an energy donor and acceptor is within 100 Å. The commercial QDs involved in the current work have large size due to the presence of ZnS shells, protective polymer layers, and streptavidin linkers. The radius of QDs is ∼75 Å, and the center-to-center distance between two adjacent QDs in the QD−SWCNT conjugates cannot be less than 150 Å (Figure 5). Therefore, FRET from QD to QD is unlikely to be present in the QD−SWCNT conjugates. Apart from this theoretical limitation of FRET, we carried out two sets of control experiments in order to examine the possibility that FRET from QDs to QDs is involved in the current work. The possibility of FRET from smaller to larger QDs was investigated by two experimental approaches: (1) by increasing the distance between QDs in a QD−SWCNT conjugate and (2) by conjugating QDs with distinctly different sizes to the same SWCNT. These two possibilities were examined based on eq 1, according to which FRET is highly sensitive to donor−acceptor distance (distance between adjacent QDs) and overlap between emission spectrum of a donor (smaller QD) and absorption spectrum of an acceptor (bigger QD).

From AFM imaging (Figures 1B and 2B) we identified that the distance between QDs can be increased by decreasing the

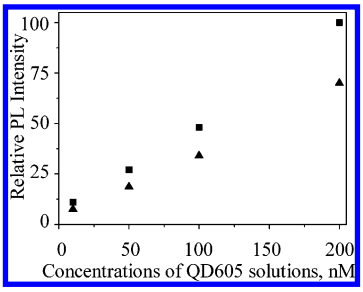

Figure 7. Relative PL intensities of (▲) QD605-SWCNT conjugates prepared from QD605 solutions with 200, 100, 50, and 10 nM concentrations, and (■) mixtures of QD605 and aniline-functionalized SWCNT solutions containing 200, 100, 50, and 10 nM QD605. PL intensities of QD605-SWCNT were always lower than that of nonconjugated QD605 irrespective of the concentration of QD605 used in the conjugation reactions.

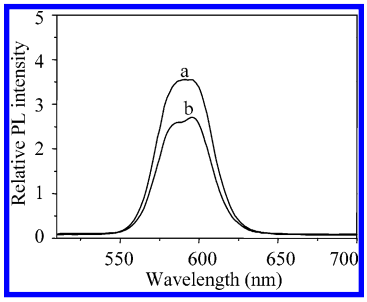

Figure 8. PL spectra of (a) a mixture of QD585 and QD605 in the presence of aniline-functionalized SWCNT and (b) mixed QD−SWCNT conjugates.

the concentration of QD solutions used in the conjugation reactions. We prepared four types of QD605-SWCNT conjugates with different inter-QDs distances for examining the distance dependence of FRET efficiency. The four types of QD605-SWCNT conjugates were prepared from 200, 100, 50, and 10 nM QD605 solutions. The PL intensities of the four samples were compared with that of a mixture of QD605 and aniline-functionalized SWCNT containing the same concentrations of QD605. The relative PL intensities of the four QD−SWCNT conjugates and that of the mixtures of QD605 and aniline-functionalized SWCNT are shown in Figure 7. We observed decreased PL intensities of QDs in QD605-SWCNT in all the four samples compared the nonconjugated QDs. However, quenching of the PL intensity was constant in all the four samples (30 ± 3%) and independent of the distance between QDs on SWCNT. In other words, quenching of the PL intensities of QDs was observed even though the distances between adjacent QDs were much larger than the theoretical limit of FRET. This simply means that FRET from QD to QD is not involved in the quenching of the PL intensities and lifetimes of QDs in QD−SWCNT conjugates. On the other hand, quenching of the PL is inherent to the QD−SWCNT conjugates, probably due to FRET from QD to SWCNT. The possibility of FRET from smaller to bigger QDs was also examined by integrating distinctly smaller and bigger QDs to the same SWCNT and investigating the relative PL intensities of the smaller and bigger QDs in the QD−SWCNT conjugate. The sample involved in this investigation was a mixed QD−SWCNT conjugate containing both QD585 and QD605. The PL spectrum of the mixed QD−SWCNT conjugate is shown in Figure 8 (trace b). The PL spectrum of a solution containing a mixture of QD585, QD605, and aniline-functionalized SWCNT is also shown in Figure 8 (trace a) for reference. The relative PL intensities of QD585 and QD605 are comparable in traces a and b. This means that FRET from QD585 to QD605 is negligible in the mixed QD−SWCNT conjugates. The low PL intensity of the mixed QD−SWCNT conjugate (trace b in Figure 8) compared to trace a in Figure 8 is understandable in terms of FRET from QD to SWCNT. This observation is similar to the quenching of the PL intensities observed in Figure 4A and B. If FRET from QD585 to QD605 was significant in the mixed QD−SWCNT conjugates, a considerable reduction in the PL intensity of QD585 (∼585 nm) and a corresponding enhancement in the PL intensity of QD605 (∼600 nm) were expected. Indeed, we observed that the PL intensity of the mixed QD−SWCNT at 585 nm is slightly lower than that at 605 nm. This is accounted for in terms of the relatively small size of QD585 which in turn probably provided slightly higher FRET from QD585 to SWCNT compared to the FRET from QD605 to SWCNT. These observations confirmed that FRET from QD to QD is not significant in the current work that and the reduced PL intensities and lifetimes are inherent to QD−SWCNT conjugates due to FRET from QD to SWCNT.

Conclusion

The current work demonstrated the preparation of linear conjugates of QDs on SWCNT, control of the distribution of QDs on SWCNT using a simple chemical conjugation reaction, and effect of conjugation of QDs to SWCNT on the PL properties of QDs. We observed considerable quenching of the PL intensity and lifetime of QDs when conjugated to SWCNT. We attributed the quenching of the PL intensity and lifetime to FRET from QDs to SWCNT. From control experiments involving QD−SWCNT conjugates with different size and density of QDs we identified that inter-QD FRET is not important when QDs having larger diameters are close-packed into hierarchical structures. However, based on the current work we are unable to exclude the contribution of other factors such as electron transfer from QDs to SWCNT and destabilization of excited states in QDs to the quenching of the PL intensity and lifetime in QD−SWCNT conjugates. Investigations of PL lifetime and intermittency characteristics of single QDs attached to single SWCNT would be helpful to understand such possibilities. QD- and SWCNT-based hierarchical structures are promising materials for optoelectronic and photovoltaic applications. In this perspective easy preparation of QD−SWCNT conjugates and controlled distribution of QDs on SWCNT are interesting. Furthermore, the PL quenching of QDs in QD−SWCNT conjugates is important to be considered during the nanofabrication of QD- and SWCNT-based hybrid materials.

Acknowledgment. V.B. and M.I. are thankful to the Grant-in-Aid for Scientific Research (KAKENHI-17034068) in Priority Area 'Molecular Nano Dynamics' from the Ministry of Education, Science, and Culture, Japan.

References and Notes

(1) Coe-Sullivan, S.; Woo, W. K.; Steckel, J. S.; Bawendi, M. G.; Bulovic, V. *Org. Electron.* **2003**, *4*, 123−130.

(2) Grebinski, J. W.; Richter, K. L.; Zhang, J.; Kosel, T. H.; Kun, M. K. *J. Phys. Chem. B* **2004**, *108*, 9745−9751.

(3) Tang, Z. Y.; Kotov, N. A.; Giersig, M. *Science* **2002**, *297*, 237−240.

(4) Shin, K.; Leach, K. A.; Goldbach, J. T.; Kim, D. H.; Jho, J. Y.; Tuominen, M.; Hawker, C. J.; Russell, T. P. *Nano Lett.* **2002**, *2*, 933−936.

(5) Alivisatos, A. P. *Science* **1996**, *271*, 933−937.

(6) Pacholski, C.; Kornowski, A.; Weller, H. *Angew. Chem., Int. Ed.* **2002**, *41*, 1188− 1191.

(7) Collins, P. G.; Zettl, A.; Bando, H.; Thess, A.; Smalley, R. E. *Science* **1997**, *278*, 100−103.

(8) Kong, J.; Franklin, N. R.; Zhou, C. W.; Chapline, M. G.; Peng, S.; Cho, K. J.; Dai, H. J. *Science* **2000**, *287*, 622−625.

(9) Duan, X. F.; Huang, Y.; Cui, Y.; Wang, J. F.; Lieber, C. M. *Nature* **2001**, *409*, 66−69.
(10) Judeinstein, P.; Sanchez, C. *J. Mater. Chem.* **1996**, *6*, 511−525.
(11) Chu, Y. W.; Hu, J. H.; Yang, W. L.; Wang, C. C.; Zhang, J. Z. *J. Phys. Chem. B* **2006**, *110*, 3135−3139.
(12) Liu, K.; Nogues, J.; Leighton, C.; Masuda, H.; Nishio, K.; Roshchin, I. V.; Schuller, I. K. *Appl. Phys. Lett.* **2002**, *81*, 4434−4436.
(13) Hu, J. T.; Odom, T. W.; Lieber, C. M. *Acc. Chem. Res.* **1999**, *32*, 435−445.
(14) Thomas, K. G.; Barazzouk, S.; Ipe, B. I.; Joseph, S. T. S.; Kamat, P. V. *J. Phys. Chem. B* **2004**, *108*, 13066−13068.
(15) Chaudhary, S.; Ozkan, M.; Chan, W. C. W. *Appl. Phys. Lett.* **2004**, *84*, 2925−2927.
(16) Vlasov, Y. A.; Yao, N.; Norris, D. J. *Adv. Mater.* **1999**, *11*, 165−169.
(17) Murray, C. B.; Kagan, C. R.; Bawendi, M. G. *Science* **1995**, *270*, 1335−1338.
(18) Mattoussi, H.; Mauro, J. M.; Goldman, E. R.; Anderson, G. P.; Sundar, V. C.; Mikulec, F. V.; Bawendi, M. G. *J. Am. Chem. Soc.* **2000**, *122*, 12142−12150.
(19) Ravindran, S.; Bozhilov, K. N.; Ozkan, C. S. *Carbon* **2004**, *42*, 1537−1542.
(20) Mitchell, G. P.; Mirkin, C. A.; Letsinger, R. L. *J. Am. Chem. Soc.* **1999**, *121*, 8122− 8123.
(21) Alivisatos, A. P.; Johnsson, K. P.; Peng, X. G.; Wilson, T. E.; Loweth, C. J.; Bruchez, M. P.; Schultz, P. G. *Nature* **1996**, *382*, 609−611.
(22) Lee, S. W.; Mao, C. B.; Flynn, C. E.; Belcher, A. M. *Science* **2002**, *296*, 892−895.
(23) Hull, K. L.; Grebinski, J. W.; Kosel, T. H.; Kuno, M. K. *Chem. Mater.* **2005**, *17*, 4416−4425.
(24) Hulteen, J. C.; Martin, C. R. *J. Mater. Chem.* **1997**, *7*, 1075−1087.
(25) Biju, V.; Sudeep, P. K.; Thomas, K. G.; George, M. V.; Barazzouk, S.; Kamat, P. V. *Langmuir* **2002**, *18*, 1831−1839.
(26) Corriu, R. J. P. *Angew. Chem., Int. Ed.* **2000**, *39*, 1376−1398.
(27) Subramanian, V.; Wolf, E. E.; Kamat, P. V. *J. Am. Chem. Soc.* **2004**, *126*, 4943− 4950.
(28) Biju, V.; Barazzouk, S.; Thomas, K. G.; George, M. V.; Kamat, P. V. *Langmuir* **2001**, *17*, 2930−2936.
(29) Banfi, G.; Degiorgio, V.; Ricard, D. *Adv. Phys.* **1998**, *47*, 447−510.
(30) Coe-Sullivan, S.; Woo, W. K.; Bawendi, M. G.; Bulovic, V. *Nature* **2002**, *420*, 800−803.
(31) Klein, D. L.; Roth, R.; Lim, A. K. L.; Alivisatos, A. P.; McEuen, P. L. *Nature* **1997**, *389*, 699−701.
(32) Loss, D.; DiVincenzo, D. P. *Phys. Rev. A* **1998**, *57*, 120−126.
(33) Michler, P.; Kiraz, A.; Becher, C.; Schoenfeld, W. V.; Petroff, P. M.; Zhang, L. D.; Hu, E.; Imamoglu, A. *Science* **2000**, *290*, 2282−2285.
(34) Alivisatos, A. P. *J. Phys. Chem.* **1996**, *100*, 13226−13239.
(35) Biju, V.; Makita, Y.; Sonoda, A.; Yokoyama, H.; Baba, Y.; Ishikawa, M. *J. Phys. Chem. B* **2005**, *109*, 13899−13905.
(36) Dabbousi, B. O.; RodriguezViejo, J.; Mikulec, F. V.; Heine, J. R.; Mattoussi, H.; Ober, R.; Jensen, K. F.; Bawendi, M. G. *J. Phys. Chem. B* **1997**, *101*, 9463−9475.
(37) Klimov, V. I.; Mikhailovsky, A. A.; Xu, S.; Malko, A.; Hollingsworth, J. A.; Leatherdale, C. A.; Eisler, H. J.; Bawendi, M. G. *Science* **2000**, *290*, 314−317.
(38) Leatherdale, C. A.; Bawendi, M. G. *Phys. Rev. B* **2001**, *63*, 165315.
(39) Murray, C. B.; Norris, D. J.; Bawendi, M. G. *J. Am. Chem. Soc.* **1993**, *115*, 8706− 8715.
(40) Nirmal, M.; Brus, L. *Acc. Chem. Res.* **1999**, *32*, 407−414.
(41) Peng, Z. A.; Peng, X. G. *J. Am. Chem. Soc.* **2002**, *124*, 3343−3353.
(42) Qu, L. H.; Peng, Z. A.; Peng, X. G. *Nano Lett.* **2001**, *1*, 333−337.
(43) Sharma, S. N.; Pillai, Z. S.; Kamat, P. V. *J. Phys. Chem. B* **2003**, *107*, 10088−10093.
(44) Talapin, D. V.; Mekis, I.; Gotzinger, S.; Kornowski, A.; Benson, O.; Weller, H. *J. Phys. Chem. B* **2004**, *108*, 18826−18831.
(45) Zhang, J. Z. *Acc. Chem. Res.* **1997**, *30*, 423−429.
(46) Azamian, B. R.; Coleman, K. S.; Davis, J. J.; Hanson, N.; Green, M. L. H. *Chem. Commun.* **2002**, 366−367.
(47) Banerjee, S.; Wong, S. S. *Chem. Commun.* **2004**, 1866−1867.
(48) Banerjee, S.; Wong, S. S. *Adv. Mater.* **2004**, *16*, 34−37.
(49) Ishibashi, K.; Suzuki, M.; Toratani, K.; Ida, T.; Aoyagi, Y. *Physica E* **2003**, *16*, 35− 41.
(50) Landi, B. J.; Castro, S. L.; Ruf, H. J.; Evans, C. M.; Bailey, S. G.; Raffaelle, R. P. *Sol. Ennergy Mater. Sol. Cells* **2005**, *87*, 733−746.
(51) Park, J. W.; Choi, J. B.; Yoo, K. H. *Appl. Phys. Lett.* **2002**, *81*, 2644−2646.
(52) Ravindran, S.; Chaudhary, S.; Colburn, B.; Ozkan, M.; Ozkan, C. S. *Nano Lett.* **2003**, *3*, 447−453.
(53) Suzuki, M.; Ishibashi, K.; Ida, T.; Aoyagi, Y. *Jpn. J. Appl. Phys.* **2001**, *40*, 1915− 1917.
(54) Banerjee, S.; Kahn, M. G. C.; Wong, S. S. *Chem. Eur. J.* **2003**, *9*, 1899−1908.
(55) Haremza, J. M.; Hahn, M. A.; Krauss, T. D.; Chen, S.; Calcines, J. *Nano Lett.* **2002**, *2*, 1253−1258.
(56) Chaudhary, S.; Kim, J. H.; Singh, K. V.; Ozkan, M. *Nano Lett.* **2004**, *4*, 2415−2419.
(57) Banerjee, S.; Hemraj-Benny, T.; Wong, S. S. *Adv. Mater.* **2005**, *17*, 17−29.
(58) Dyke, C. A.; Tour, J. M. *J. Am. Chem. Soc.* **2003**, 125, 1156−1157.
(59) Dyke, C. A.; Tour, J. M. *Nano Lett.* **2003**, 3, 1215−1218.
(60) Lakowicz, J. R. *Principles of Fluorescence Spectroscopy*; Plenum Press: New York 1986.
(61) Clapp, A. R.; Medintz, I. L.; Mattoussi, H. *ChemPhysChem* **2006**, *7*, 47−57 and references therein.
(62) Kagan, C. R.; Murray, C. B.; Bawendi, M. G. *Phys. Rev. B* **1996**, *54*, 8633−8643.
(63) Clapp, A. R.; Medintz, I. L.; Fisher, B. R.; Anderson, G. P.; Mattoussi, H. *J. Am. Chem. Soc.* **2005**, *127*, 1242−1250.
(64) Clapp, A. R.; Medintz, I. L.; Mauro, J. M.; Fisher, B. R.; Bawendi, M. G.; Mattoussi, H. *J. Am. Chem. Soc.* **2004**, *126*, 301−310.
(65) Hohng, S.; Ha, T. *Chem. Phys. Chem.* **2005**, *6*, 956−960.
(66) Medintz, I. L.; Konnert, J. H.; Clapp, A. R.; Stanish, I.; Twigg, M. E.; Mattoussi, H.; Mauro, J. M.; Deschamps, J. R. *Proc. Natl. Acad. Sci. U.S.A.* **2004**, *101*, 9612−9617.
(67) Muller, F.; Gotzinger, S.; Gaponik, N.; Weller, H.; Mlynek, J.; Benson, O. *J. Phys. Chem. B* **2004**, *108*, 14527−14534.
(68) Nagasaki, Y.; Ishii, T.; Sunaga, Y.; Watanabe, Y.; Otsuka, H.; Kataoka, K. *Langmuir* **2004**, *20*, 6396−6400.
(69) Oh, E.; Hong, M. Y.; Lee, D.; Nam, S. H.; Yoon, H. C.; Kim, H. S. *J. Am. Chem. Soc.* **2005**, *127*, 3270−3271.